AIAA 81-4273

Analysis of Turbulent Boundary Layer on Cascade and Rotor Blades of Turbomachinery

B. Lakshminarayana* and T. R. Govindan†
The Pennsylvania State University, University Park, Pa.

The momentum integral technique for predicting the boundary-layer growth in three-dimensional flow has been extended to include the entrainment equation as the closure model. The numerical solution is compared with the cascade, inducer, compressor, and fan rotor blade data from various sources. The agreement is found to be excellent in all cases, with the exception of the separated flow. Both the momentum thickness and the limiting streamline angle predicted from this analysis compare well with the measured data for a rotor blade. The technique is extremely useful in engineering design, analysis, and performance prediction.

Nomenclature

c	= chord length
C_L	= lift coefficient
C_E	= entrainment coefficient
C_f	= skin friction coefficient
F	= entrainment rate [Eq. (11)]
h_1,h_2,h_3	= scale factors of the coordinate system
H	= shape factor [Eq. (5)]
$H_{\delta-\delta_1}$	= Head's form of the shape factor
J,K,M,N	= functions of the shape factor [defined in Eq. (9)]
N,Ω	= rpm, angular velocity
R	= r/r_t, where r_t is the tip radius
R_e	= Reynolds number based on upstream velocity and blade chord at midradius
$R_{\theta_{11}}$	= Reynolds number based on boundary-layer edge velocity and the local momentum thickness θ_{11}
(s,n,r)	= streamwise, normal, and radial directions in the curvilinear coordinates (Fig. 1)
U_e	= streamwise velocity at the edge of the boundary layer
u,v,w	= streamwise, normal, and radial components of velocity
x	= chordwise distance from the leading edge
λ	= stagger angle
$\alpha_\omega,\epsilon_\omega$	= limiting streamline angle, $\tan\alpha_\omega$
δ	= boundary-layer thickness
δ_1,δ_2	= displacement thickness [defined in Eq. (4)]
$\theta_{11},\theta_{12},\theta_{21},\theta_{22}$	= momentum thicknesses [defined in Eq. (4)]

Subscripts

s,n,r	= values in streamwise, normal, and radial directions, respectively

Introduction

A KNOWLEDGE of the properties of the blade boundary layer on rotor blades is essential for the prediction of the efficiency, aerodynamic, and acoustic performance of a turbomachinery rotor. The boundary layer that develops on rotor blades is not two-dimensional. The rotation and the curvature effects produce three-dimensionality in the flow with appreciable radial velocities. Furthermore, the Coriolis and centrifugal force fields modify the skin friction stress on the blade. These effects have to be included in the analysis of the boundary layer developing on a rotor blade. The boundary-layer parameters that are of interest are the displacement and momentum thicknesses, the limiting streamline angle, and the skin friction coefficient. The limiting streamline angle is the angle of the streamline (measured as a deviation from the inviscid streamline) as the blade surface is approached.

There are two methods commonly used to calculate the flow properties in the boundary layer—the differential method and the momentum integral technique. Finite-difference techniques are employed in the differential method to compute the details of the flow in the boundary layer. While this is necessary in understanding the nature of the boundary layer, the calculations are complex, time consuming, and difficult to incorporate into the design, analysis, and performance prediction of a turbomachine. Momentum integral techniques, on the other hand, provide the gross properties of the boundary layer. In most cases this is all that is required in the preliminary design and analysis to correct the inviscid flow in the blade passage for the effects of the blade boundary layer. The momentum integral method provides a quick estimate of the boundary-layer parameters and is easily coupled to inviscid flow calculation routines. The chief virtue of an integral method lies in the implicit and global manner in which the effects of turbulence are incorporated.

Several researchers have utilized this method for the three-dimensional boundary-layer calculation over different flow configurations. Cumpsty and Head,[1] Thompson and MacDonald,[2] and Smith,[3] among others, have developed the method for flow over an infinite swept wing. Mager[4] has derived generalized integral equations, including those for rotating systems. Lakshminarayana et al.[5] and Anand and Lakshminarayana[6,7] have applied the method to the three-dimensional boundary on a rotating helical blade and inducer channel, respectively.

The present method is an extension of the above methods to a turbomachinery rotor. In a turbomachine rotor, the effects of rotation, curvature, and pressure gradients are all important. Furthermore, the finite extent of the blade height requires suitable boundary conditions to be prescribed on both the hub and the casing walls. A method incorporating these features is presented here, and results obtained from its application are compared with the experimental data. The entrainment equation is included as a closure to the momentum equations.

Received Nov. 17, 1980; revision received March 30, 1981.

*Director, Computational Fluid Dynamics Studies and Professor, Aerospace Engineering. Associate Fellow AIAA.
†Graduate Assistant in Aerospace Engineering.

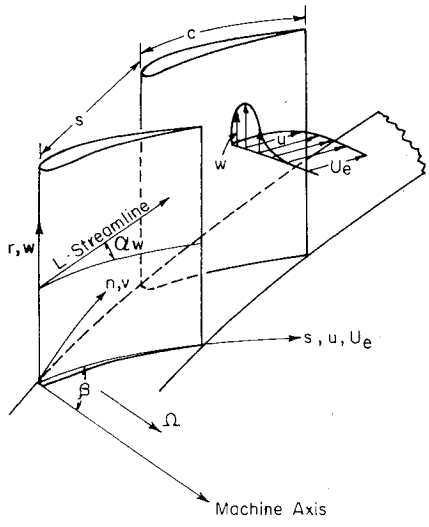

Fig. 1 Curvilinear coordinate system and notations used.

Boundary-Layer Analysis

Momentum Integral Equations

The momentum integral equations for the three-dimensional boundary layer of an incompressible fluid have been derived by many researchers.[1-7] The technique presented in this paper is an extension of the earlier methods developed by Lakshminarayana et al.[5] for a rotating helical blade and Anand and Lakshminarayana[6] for a rotating helical channel. The technique includes the effect of three-dimensional inviscid-external flow. The new features presented in this paper include the incorporation of a three-dimensional entrainment equation and coupling of the three-dimensional inviscid computer program due to Katsanis and McNally[8] with the momentum integral program for boundary-layer calculation.

The momentum integral equations are obtained by integrating the boundary-layer equations in the normal direction. The resulting two momentum integral equations (one in the mainstream, the other in radial flow direction) are reduced to two first-order, partial-differential equations using a power law profile for the mainstream velocity, Mager's profile[4] for the cross flow, and a skin friction relation based on the experimental data of Anand and Lakshminarayana,[6] which is a modification of Ludwieg and Tillmann's[9] skin friction correlation for two-dimensional flows to three-dimensional turbulent boundary layers with pressure gradients, including the effect of rotation. The exponent of the power law for the streamwise velocity component is a function of the local shape parameter (H), which is defined as the ratio of streamwise displacement thickness to streamwise momentum thickness. It thus represents the shape of the streamwise velocity profile.

The coordinate system employed and some of the notations used are shown in Fig. 1, where s is the coordinate in the direction of the inviscid streamline at the edge of the boundary layer, n is normal to s and the blade surface, and r is normal to s and n along the blade surface. The momentum integral equation in s and r directions in the rotating orthogonal coordinate system is given, respectively, by

$$\frac{1}{h_1}\frac{\partial\theta_{11}}{\partial s}+\frac{2}{U_e}\frac{1}{h_1}\frac{\partial U_e}{\partial s}\theta_{11}+\frac{1}{h_3}\frac{\partial\theta_{12}}{\partial r}+\frac{2}{U_e}\frac{1}{h_3}\frac{\partial U_e}{\partial r}\theta_{12}$$
$$+\frac{1}{U_e}\frac{1}{h_1}\frac{\partial U_e}{\partial s}\delta_1+\frac{1}{U_e}\frac{1}{h_3}\frac{\partial U_e}{\partial r}\delta_2+\frac{1}{h_1h_3}\frac{\partial h_3}{\partial s}(\theta_{11}-\theta_{22})$$
$$+\frac{1}{h_1h_3}\frac{\partial h_1}{\partial r}(\theta_{12}+\theta_{21})-2\delta_2\frac{\Omega_n}{U_e}=\frac{C_{fs}}{2} \tag{1}$$

and

$$\frac{1}{h_1}\frac{\partial\theta_{21}}{\partial s}+\frac{2}{U_e}\frac{1}{h_1}\frac{\partial U_e}{\partial s}\theta_{21}+\frac{1}{h_3}\frac{\partial\theta_{22}}{\partial r}+\frac{2}{U_e}\frac{1}{h_3}\frac{\partial U_e}{\partial r}\theta_{22}$$
$$+\frac{1}{h_1h_3}\frac{\partial h_3}{\partial s}(\theta_{21}+\theta_{12}+\delta_2)+\frac{1}{h_1h_3}\frac{\partial h_1}{\partial r}(\theta_{22}-\theta_{11}-\delta_1)$$
$$+2\delta_1\frac{\Omega_n}{U_e}=\frac{C_{fr}}{2} \tag{2}$$

where U_e is the inviscid freestream velocity. The usual assumption that the boundary layer is thin compared to the radius of curvature of the blade surface has been made ($h_2=1$).

An arc length ds in this coordinate system with the thin-layer approximation is given by

$$dS=(h_1ds)^2+dn^2+(h_3dr)^2 \tag{3}$$

The various boundary-layer thicknesses are defined as

$$\theta_{11}=\int_0^\delta\frac{u}{U_e}\left(1-\frac{u}{U_e}\right)dn \tag{4a}$$

$$\theta_{12}=\int_0^\delta\frac{w}{U_e}\left(1-\frac{u}{U_e}\right)dn \tag{4b}$$

$$\theta_{21}=-\int_0^\delta\frac{uw}{U_e^2}dn \tag{4c}$$

$$\theta_{22}=-\int_0^\delta\left(\frac{w}{U_e}\right)^2dn \tag{4d}$$

$$\delta_1=\int_0^\delta\left(1-\frac{u}{U_e}\right)dn \tag{4e}$$

$$\delta_2=-\int_0^\delta\frac{w}{U_e}dn \tag{4f}$$

A power law type of velocity profile is assumed for the mainstream velocity profile.

$$u/U_e=(n/\delta)^{(H-1)/2} \tag{5}$$

where H is the local shape factor.

The assumed cross-flow profile is from Ref. 4:

$$w/u=\epsilon_w(1-n/\delta)^2 \tag{6}$$

where ϵ_w is the limiting streamline parameter ($\tan\alpha_w$).

Equations (1) and (2) can now be written in terms of the four parameters θ_{11}, ϵ_w, H, and C_{fs}.

$$\frac{1}{h_1}\frac{\partial\theta_{11}}{\partial s}+(2+H)\frac{1}{h_1}\theta_{11}\frac{1}{U_e}\frac{\partial U_e}{\partial s}+\left\{\frac{2}{h_3}J\epsilon_w\theta_{11}+\frac{L\epsilon_w\theta_{11}}{h_3}\right\}$$
$$\times\frac{1}{U_e}\frac{\partial U_e}{\partial r}+\frac{1}{h_3}\frac{\partial}{\partial r}(J\epsilon_w\theta_{11})+\frac{1}{h_1h_3}\frac{\partial h_3}{\partial s}(\theta_{11}-M\epsilon_w^2\theta_{11})$$
$$+\frac{1}{h_1h_3}\frac{\partial h_1}{\partial r}(J\epsilon_w\theta_{11}+N\epsilon_w\theta_{11})-2\frac{\Omega_n}{U_e}(L\epsilon_w\theta_{11})=\frac{C_{fs}}{2} \tag{7}$$

and

$$\frac{1}{h_1}\frac{\partial}{\partial s}(N\epsilon_w\theta_{11})+\frac{1}{h_1}\frac{2}{U_e}\frac{\partial U_e}{\partial s}(N\epsilon_w\theta_{11})+\frac{1}{h_3}\frac{\partial}{\partial r}(M\epsilon_w^2\theta_{11})+\frac{2}{U_e}\frac{1}{h_3}\frac{\partial U_e}{\partial r}(M\epsilon_w^2\theta_{11})+\frac{1}{h_1h_3}\frac{\partial h_3}{\partial s}(N\epsilon_w\theta_{11}+J\epsilon_w\theta_{11}+L\epsilon_w\theta_{11})+\frac{1}{h_1h_3}\frac{\partial h_1}{\partial r}(M\epsilon_w^2\theta_{11}-\theta_{11}-\theta_{11}H)+2\frac{\Omega_n}{U_e}H\theta_{11}=\frac{\epsilon_w C_{fs}}{2} \tag{8}$$

where

$$J=\frac{\theta_{12}}{\epsilon_w\theta_{11}}=\frac{(30.0+14H)}{(H+2)(H+3)(H+5)} \tag{9a}$$

$$L=\frac{\delta_2}{\epsilon_w\theta_{11}}=-\frac{16H}{(H-1)(H+3)(H+5)} \tag{9b}$$

$$M=\frac{\theta_{22}}{\epsilon_w^2\theta_{11}}=\frac{-24}{(H-1)(H+2)(H+3)(H+1)} \tag{9c}$$

$$N=\frac{\theta_{21}}{\epsilon_w\theta_{11}}=\frac{-2}{(H-1)(H+2)} \tag{9d}$$

The skin-friction relation for flows with pressure gradients and rotation effects is based on the experimental data for a turbulent boundary layer in a rotating channel developed by Anand and Lakshminarayana.[6,7]

$$C_{fs}=0.172R_{\theta_{11}}^{-0.268}10^{-0.678H}(1+B_1\sqrt{\epsilon_w(s-s_t)/c}) \tag{10}$$

This correlation is a modified version of the correlation developed by Ludwieg and Tillmann.[9] B_1 is a constant; a value of 0.52, suggested by Anand and Lakshminarayana,[6] is used; $R_{\theta_{11}}$ is the Reynolds number, based on the streamwise velocity at the edge of the boundary layer and the streamwise momentum thickness θ_{11}; and s_t is the distance between the leading edge and the transition point along the s direction.

Closure Model—Entrainment Equation

In turbomachinery blade passages, the flow experiences large pressure gradients. These pressure gradients cause large changes in velocity profiles and consequently in the shape parameter H. The variation of H cannot be neglected and an additional equation is required. Out of the available auxiliary equations, only the "energy integral equation" and the "entrainment equation" have been found suitable for the turbulent boundary layers.[10] The former involves more empiricism in calculating the dissipation integral term, and assumes the shear stress distribution in the turbulent boundary layer. Since the shear stress variation differs largely from flow to flow, especially those under the influence of rotation and curvature, the entrainment equation rather than energy integral equation is used. The entrainment equation is derived from the concept that a turbulent boundary layer grows by a process of "entrainment" of the inviscid fluid at the edge of the boundary layer into the turbulent region and has been found to give good predictions in a variety of flows as demonstrated by Kline et al.[10] The entrainment equation by Head[11] has been extended by Nash and Patel[12] for a three-dimensional flow. The entrainment equation is obtained from the integration of the continuity equation from the blade surface ($y=0$) to the edge of the boundary layer ($y=\delta$). The continuity equation is the same both in the rotating and stationary coordinate system (s, n, r).

The entrainment equation for the rotor boundary layer in the coordinate system used in this paper (Fig. 1) can be shown to be

$$\frac{1}{h_1}\frac{\partial}{\partial s}(\delta-\delta_1)+(\delta-\delta_1)\left\{\frac{1}{h_1}\frac{1}{U_e}\frac{\partial U_e}{\partial s}+\frac{1}{h_1h_3}\frac{\partial h_3}{\partial s}\right\}-\frac{1}{h_3}\frac{\partial\delta_2}{\partial r}-\delta_2\left\{\frac{1}{h_3}\frac{1}{U_e}\frac{\partial U_e}{\partial r}+\frac{1}{h_1h_3}\frac{\partial h_1}{\partial r}\right\}=F(H_{\delta-\delta_1}) \tag{11}$$

where δ_1 and δ_2 are displacement thickness parameters in streamwise and cross-flow directions, respectively, and are defined in Eq. (4) and $H_{\delta-\delta_1}=(\delta-\delta_1)/\theta_{11}$. F on the right-hand side represents the volume flow rate per unit area through the surface $\delta(s,r)$ and is the rate of entrainment of inviscid external flow into the boundary layer.

The entrainment process is a highly complex and inherently unsteady phenomena and its direct measurement is difficult. The entrainment rate depends both on the mean flow parameters, such as the streamwise velocity defect, the rate of boundary-layer growth, freestream velocity, displacement thickness, etc., as well as on the turbulent quantities, such as turbulence intensities and stresses in the outer layer. The streamwise velocity defect, in turn, is directly related to freestream velocity, the shape factor, the magnitude of cross flow, and the blockage effects due to confinement of external inviscid flow in the channel. An empirical correlation for the entrainment function F for three-dimensional flow is not yet available. Hence, the entrainment function F due to Head[11] for two-dimensional flow is used in the present analysis. The function is given by

$$F(H_{\delta-\delta_1})=0.0306(H_{\delta-\delta_1}-3.0)^{-0.653} \tag{12}$$

It is assumed that the variation of the entrainment rate with $H_{\delta-\delta_1}$ follows the same relationship for three-dimensional flows.

Equation (11) is written in a form similar to Eqs. (7) and (8)

$$\frac{1}{h_1}\frac{\partial}{\partial s}(\theta_{11}H_{\delta-\delta_1})+(\theta_{11}H_{\delta-\delta_1})\left\{\frac{1}{h_1}\frac{1}{U_e}\frac{\partial U_e}{\partial s}+\frac{1}{h_1h_3}\frac{\partial h_3}{\partial s}\right\}-\frac{1}{h_3}\frac{\partial}{\partial r}(L\epsilon_w\theta_{11})-(L\epsilon_w\theta_{11})\left\{\frac{1}{h_3}\frac{1}{U_e}\frac{\partial U_e}{\partial r}+\frac{1}{h_1h_3}\frac{\partial h_1}{\partial r}\right\}=F(H_{\delta-\delta_1}) \tag{13}$$

Equations (7), (8), and (13) are to be solved for θ_{11}, ϵ_w, and H ($H_{\delta-\delta_1}$ is related to H) with the prescribed boundary conditions. For a Cartesian system, $h_1=h_2=h_3=1$. For the cascade test cases presented later, the surface curvature is neglected ($h_1=h_3=1$), and the inviscid and the viscid flow is assumed to be two dimensional ($w=\epsilon_w=0$). Hence, only the s-momentum equation is relevant in the analysis. For the rotor blade when the surface curvature is negligible, $h_3=1$ and

$$\frac{1}{h_1}\frac{1}{h_3}\frac{\partial h_1}{\partial r}=\frac{\sin^2\lambda}{r}$$

The inviscid flowfield for a cascade is derived either from the measured blade pressure distribution or from the cascade inviscid flow prediction. The rotor inviscid flowfield [$U_e(s,r)$], which is three dimensional, is derived from the computer program developed by Katsanis and McNally.[8]

Initial conditions are prescribed for θ_{11}, ϵ_w, and H at the leading edge. θ_{11} and ϵ_w are assumed to be zero at the leading edge and an initial value of 1.4 is assumed for H. The boundary condition prescribed at the end walls is that ϵ_w is zero there.

Table 1 Details of experimental data used for testing the prediction method

No.	Test case	Reynolds number, R_e	rpm	Stagger[b] angle, deg	Spacing,[b] cm	C_L	Hub-tip ratio	Blade chord, cm	Correlation for skin-friction coefficient used, Ref.	Figs.
1	Compressor cascade 55-deg inlet angle[13]	3×10^5	—	45	10.5	0.458	—	12.38	9	2
2	Compressor cascade 62-deg inlet angle[13]	3×10^5	—	45	10.5	0.54	—	12.38	9	2
3	Turbine cascade rough blade[14]	5.6×10^5	—	56.5	11.98	4.83	—	17.50	14	3
4	Turbine cascade smooth blade[14]	5.6×10^5	—	56.5	11.98	4.83	—	17.50	9	Not shown
5	Single rotating helical blade[5]	1.75×10^6	450	81	—	0.0	0.50	181.20 at midradius	6	4a,4b
6	Rocket pump inducer blade[6,7]	1.75×10^6	450	81	56	Very small	0.50	181.20 at midradius	6	5
7	Axial flow compressor rotor blade[16,17]	3.0×10^5	1066	30	10.50	0.6	0.50	12.70-15.25	6	6,7
8	Axial flow compressor rotor blade[a] Effect of rotation[a]	3.0×10^5	1066 1280 2132			—	0.50	12.70-15.25	6	8
9	Axial flow compressor rotor blade[a] Effect of streamwise pressure gradient[a]	3.0×10^5	1066			—	0.50	12.70-15.25	6	9
10	Axial flow fan rotor blade[18,19]	3.0×10^5	1010	45	10.33	0.30	0.44	15.20	6	10,11

[a] Hypothetical compressor. [b] At midradius.

Numerical Solution

The method of solution of Eqs. (7), (8), and (13) is similar to that suggested by Mager.[4] An initial value of the shape factor is assumed at the streamwise station at which the calculation is being carried out and Eqs. (7) and (8) are solved for the momentum thickness and the limiting streamline parameter at that station. Equation (13) is now used to update the value of the shape factor. Equations (7) and (8) are solved again with the new value of the shape factor, and the procedure is repeated until the solution converges.

The application of the end wall (hub and annulus walls) boundary conditions on the limiting streamline parameter was found to cause instabilities in the numerical calculation. A possible reason for this is that the equations do not model the corner flow correctly, where both transverse gradients are important. Since this is not the region of interest of the calculation, it was found that the calculation could be stabilized by calculating the radial derivatives of the limiting streamline parameter by using the boundary conditions on the end wall and the solution domain adjacent to it (located approximately at the edge of the wall boundary layer), the equations themselves not being integrated along the end walls. Such a scheme is easily implemented using explicit-difference schemes described below.

The Gill variation of the Runge-Kutta fourth-order scheme is used to integrate Eqs. (7), (8), and (13) in the streamwise direction. A centered-difference approximation is used for the radial derivative. The method is an explicit scheme in that the radial derivatives are lagged in the calculation. Such an approach is similar to the "method of lines" approach to solving partial-differential equations. The four-step Runge-Kutta method allows the radial derivatives to be corrected at each half-step of the calculation.

For some of the simpler flow geometries considered in this paper, grid points on which the calculation was carried out were specified with the input. However, for the more complicated geometries, the grid system was carried over from the inviscid solver[8] used to calculate the pressure and velocity gradients. Such a system makes it easy to integrate the boundary-layer program with the inviscid solver. The inviscid solver used here for a rotor is that of Katsanis and McNally.[8]

The numerical scheme has shown no instability in the test cases for which the program was run. Characteristic run times for the two-dimensional boundary layers were between 1 and 2 s using 20 streamwise stations. Run times for the three-dimensional boundary layers considered were between 6 and 10 s using 20 streamwise stations and 12 radial stations. These run times are expected to be reduced further when final versions of the program are run. The program is written in FORTRAN IV and run on The Pennsylvania State University's IBM 3033 processor.

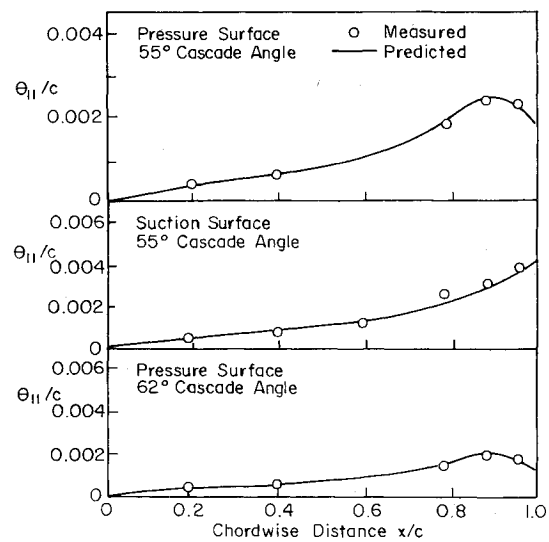

Fig. 2 Chordwise distribution of momentum thickness for a compressor cascade at inlet angles of 55 and 62 deg.[13]

Prediction and Comparison with Experimental Data

To check the analysis, assumptions, and numerical technique, the computer program was run for the two-dimensional boundary layers on cascades[13,14] and the three-dimensional boundary layers on inducer,[5-7] compressor,[16,17] and fan[18,19] rotor blades. Details of the various test cases utilized are tabulated in Table 1, including a listing of the stagger angle, Reynolds number, blade spacing, chord length, hub/tip ratio, speed, and the skin-friction correlation employed, as well as figures in which the data are presented. The

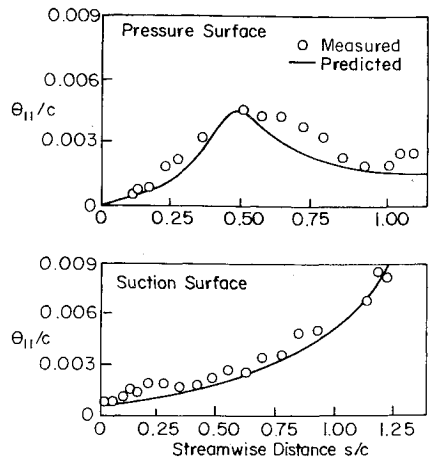

Fig. 3 Chordwise distribution of momentum thickness for a rough turbine cascade blade.[14]

prediction for the cascade cases (items 1-4) includes only the streamwise pressure or inviscid velocity gradients, while the rotor cases (items 5-10) include both the streamwise ($\partial U_e/\partial s$) and the radial gradient ($\partial U_e/\partial r$) of the inviscid streamwise velocity needed in Eqs. (7), (8), and (13).

Compressor Cascade[13]

The prediction of the momentum thickness from the authors' analysis has been compared with the measurements of Peterson[13] in a compressor cascade. The comparison for the 55 and 62 deg inlet angles is shown in Fig. 2. The measured blade pressure distribution was utilized to derive the value of U_e. The flow is two-dimensional, with $w=\epsilon_w=0$; hence, Eqs. (7) and (13) are solved. In these calculations, the Ludwieg-Tillmann law[9] was used to calculate the skin-friction coefficient and Head's entrainment equation [two-dimensional form of Eq. (13)] was utilized to close the set of equations. Predictions compare very well with the measured data on both surfaces of the 55 deg case. Of interest is the reduction in momentum thickness on the pressure surface toward the trailing edge caused by an acceleration of the flow. This trend is predicted well. Predictions are excellent in the case of the 62 deg inlet angle for the pressure surface. The suction surface of this cascade showed separation at 62 deg inlet angle; hence results from it are not shown.

Turbine Cascade[14]

The measurement by Bammert and Sandstede[14] on a rough turbine cascade blade is compared with the predictions in Fig. 3. Results shown here are for a roughness grade of 3.3×10^{-3}, and the skin-friction law suggested by Bammert and Sandstede was used. Predictions compare very well with the measured data on the suction surface. On the pressure surface, the momentum thickness predicted is lower than the measured values beyond the transition point. It is not known if this error is due to the skin-friction law used, the input pressure distributions, or the measurement errors.

The predictions of the momentum thickness growth in the case of a smooth turbine cascade blade shows very good agreement with the data (not shown). The Ludwieg-Tillmann law[9] was used to calculate the skin-friction coefficient. The transition point was specified in the input to the program, and the skin-friction coefficient for a flat plate in laminar flow was used for the initial laminar length.

Single Rotating Helical Blade[5]

Most comprehensive data on a single rotating blade of tip radius 91 cm, with a chord length of 181 cem at the mid-radius, were reported by Lakshminarayana et al.[5] The boundary-layer profile was measured at several chordwise and radial locations. The analysis from this paper is compared with their data in Fig. 4. Equations (7), (8), and (13) were solved simultaneously using Eq. (10) for the skin-friction coefficient. The asymptotic laminar solution of Banks and Gadd[15] was used to start the solution, and only the flow in the turbulent region was computed.

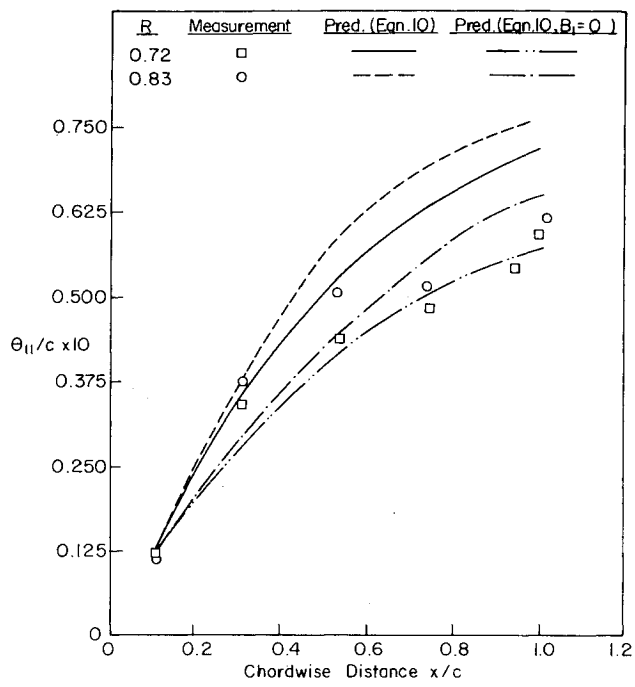

Fig. 4a Chordwise distribution of momentum thickness on a single rotating blade at $R=0.72$ and 0.83.[5]

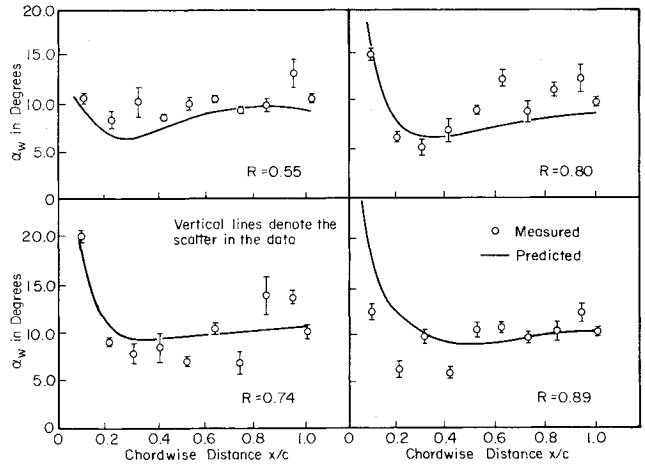

Fig. 4b Chordwise distribution of limiting streamline angle on a single rotating helical blade at $R=0.55, 0.74, 0.80, 0.89$.[5]

The momentum thickness for the rotor blade at $R=0.72$ and 0.83 is compared with the predictions in Fig. 4a. The prediction is excellent up to 0.3 chord length, beyond which the simple shear stress correlation of Ludwieg and Tillmann[9] [with $B_1=0$ in Eq. (10)] seems to work better. The comparison provides an excellent check on the ability of the analysis to predict the effects of the Coriolis and the centrifugal forces in the development of a three-dimensional turbulent boundary layer.

The limiting streamline angles at various radial and chordwise locations, measured using the ammonia-ozalid technique, are shown compared with the predictions in Fig. 4b. The vertical lines at the data points indicate the scatter in the data obtained by repetitive measurements. Considering this scatter, the agreement between the prediction and data is very good, except in the trailing-edge region (and leading-edge region for $R=0.89$). Since the present analysis includes the

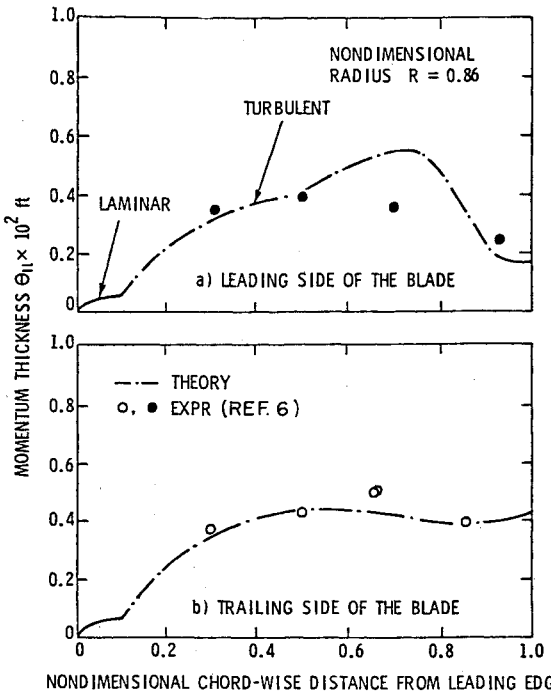

Fig. 5 Chordwise distribution of momentum thickness at $R = 0.86$ for an axial flow inducer blade.[6]

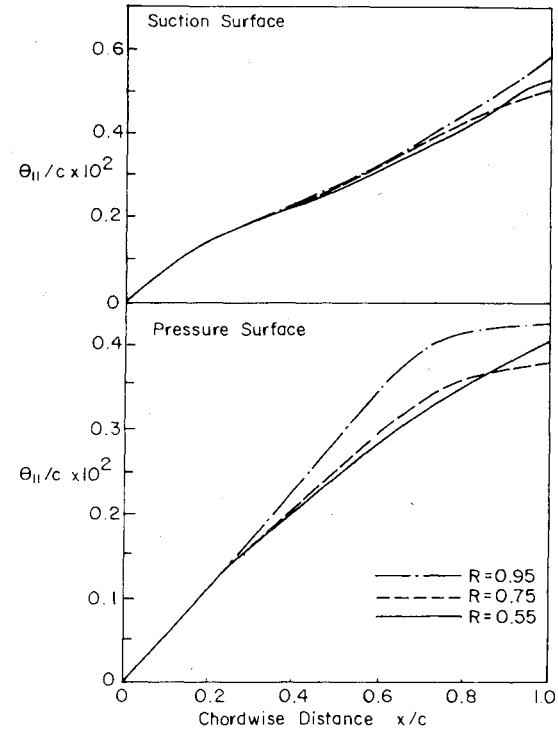

Fig. 6 Predicted chordwise distribution of momentum thickness on a compressor rotor blade at various radii.

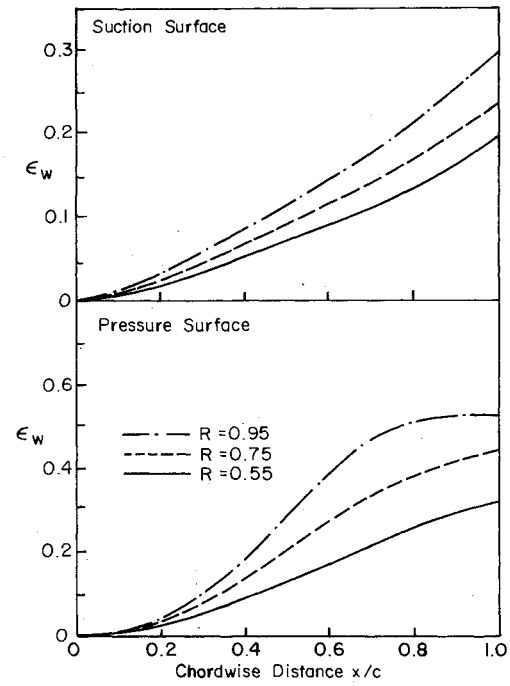

Fig. 7 Predicted chordwise distribution of ϵ_w on a compressor rotor blade at various radii.

gross effects of the hub and tip wall, the prediction is better than the ones reported in Ref. 5. Existence of large values of ϵ_w near the leading edge due to the presence of the laminar initial length is also predicted well.

Rocket Pump Inducer Rotor Blade[6,7]

Rocket pump inducers are characterized by fewer blades (three to four) of large chord length and stagger angle. A flat plate inducer was tested in air with an open throttle at The Pennsylvania State University.[6,7] Important geometrical and flow parameters of this inducer are listed in Table 1. Extensive measurement of the blade boundary-layer profile and the limiting streamline angle was carried out utilizing the boundary-layer probes and the ammonia-ozalid technique, respectively. This case corresponds to zero-pressure gradient ($H = 1.28$); hence momentum equations (7) and (8) alone provide accurate solution. The results of the analysis carried out earlier[6] are shown in Fig. 5. Comparison of the predicted and measured momentum thicknesses shows excellent agreement on both the leading and the trailing surfaces of the rotor blade, with the exception of one data point near the trailing edge. The measured limiting streamline angle is also in good agreement with the predictions, with the exception of the region near the trailing edge.[6]

The test case dealt with in this section, namely the absence of the chordwise pressure gradient but the presence of rotation and curvature effects in a long and narrow channel, provides a severe test on the model for the effect of the curvature and the rotation as well as the radial pressure gradient. Good agreement between the theory and the experiment indicate that the analysis accurately predicts these effects.

Axial Flow Compressor Rotor Blade[17]

The Axial Flow Compressor Facility, described in Ref. 16, was utilized to study the wake characteristics of a rotor blade. The compressor facility is single-stage with IGV, rotor, and stator in sequence. The rotor is 0.91 m in diameter with 21 blades. Other features of this rotor are given in Table 1. The rotor wake was measured using a triaxial hot-wire probe, rotating with the blade and traversed by a step-motor-driven traverse gear. Details of the technique and facility can be found in Refs. 16 and 17. The wake measurement at the trailing edge (axial distance from the trailing edge = 0.0104 chord) was utilized to derive the values of the momentum thickness (θ_{II}) at the trailing edge at various radii. The data on the limiting streamline angle measurement are not available.

Results obtained from the analysis of the three-dimensional turbulent boundary layer on the compressor rotor blade are shown in Figs. 6 and 7 for three radii on both the pressure and the suction surfaces. The flow is assumed to be turbulent throughout. The inviscid flow in the rotor passage was obtained by using the computer program of Katsanis and McNally.[8] Figure 6 shows the momentum thickness

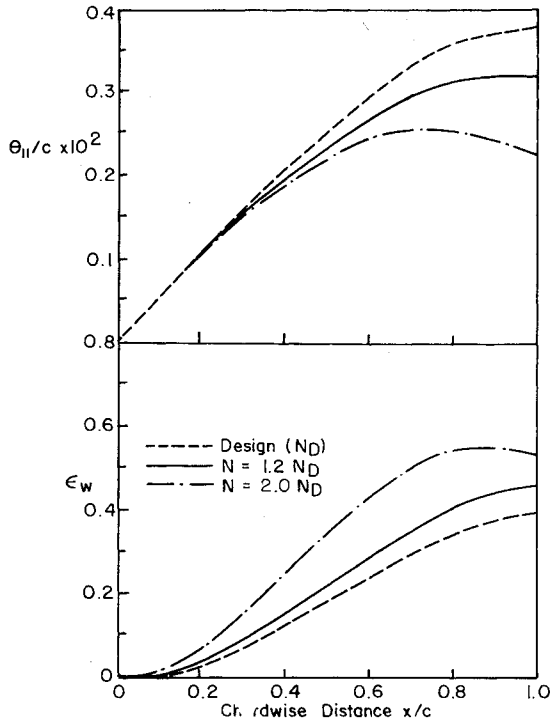

Fig. 8 Effect of rotation on the pressure surface boundary layer of a compressor rotor blade.

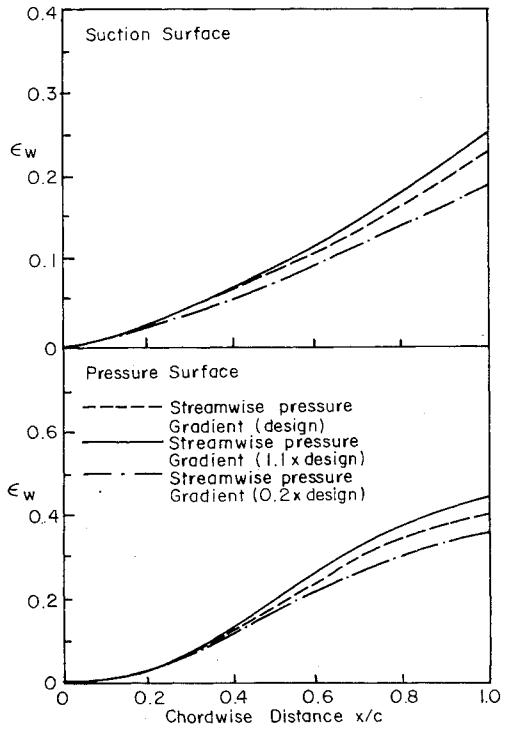

Fig. 9 Effect of streamwise pressure gradient on the limiting streamline angle for a compressor rotor blade.

Table 2 Measured and predicted values of momentum thickness for the compressor rotor[17] at the trailing edge

Predictions		Measurements[17]	
R	θ_{11}/C	R	θ_{11}/C
0.65	0.0127	0.6581	0.0115
0.80	0.0105	0.7973	0.0101
0.90	0.0110	0.9324	0.0115

distribution on the blade at various radial locations. The predictions show a large value of θ_{11} on the suction side of the blade. The momentum thickness at the trailing edge decreases from the hub toward the midradius and increases again toward the tip and attains the maximum values there. Such a trend is also seen in the measurements in the rotor wake close to the trailing edge reported in Ref. 17. No measurements are available on the blade surface. Comparisons of the momentum thickness predicted at the trailing edge with the measurements in the wake are good (Table 2). In Table 2, θ_{11} is the sum of the corresponding thicknesses on the pressure and suction surfaces. The cross flow tends to reduce the momentum thickness at the hub and increase it toward the tip. Prediction of the large growth in the boundary at the interaction region near the tip, observed by many investigators, is beyond the scope of the present analysis as the effect of the annulus wall boundary layer is not included in the analysis.

Figure 7 shows the limiting streamline angle distributions on the suction and pressure surfaces. The limiting streamline angles are greater on the pressure surface than on the suction surface. The angle increases from hub to tip. The observed trend in the distribution of ϵ_w on the two surfaces are different. The limiting streamline (α_w) angle increases continuously toward the trailing edge on the suction surface, but tends to level off on the pressure surface. This trend is probably due to the nature of the velocity and pressure gradients in the inviscid flow. It is clear that the limiting streamline angle increases continuously from a value of 11 deg at the hub to 17 deg at the tip on the suction surface. A similar trend is also observed on the pressure surface of the blade. The prediction of the radial flows inside the blade boundary layer, through the parameter ϵ_w, is very essential for the accurate estimate of the three-dimensional effects and the hub-to-tip distribution of the flow losses in turbomachinery. The analysis described in this paper could be utilized to predict such a radial distribution of losses.

Effect of Rotation for a Hypothetical Compressor

A parametric study was carried out to determine the effects of the rotation on the momentum thickness and the limiting streamline angle on a rotor blade. For the investigation of the effects of rotation, all other aerodynamic parameters (including the Reynolds number

$$\frac{1}{U_e}\frac{\partial U_e}{\partial s}, \quad \frac{1}{U_e}\frac{\partial U_e}{\partial r}, \quad U_e, C, \nu$$

and the blade pressure distribution) are held constant. The relevant parameters for this case are tabulated in Table 1 (item 8). The rotation parameter Ω_n/U_e was varied by varying the rotational speed N. The aerodynamic properties $U_e(s,r)$ are the same as that of the compressor rotor investigated earlier. This would result in a hypothetical compressor. In summary, all the aerodynamic parameters of the blade row, with the exception of Ω_n, are held constant in Eqs. (7) and (8). The results are shown in Fig. 8 for the pressure surface of the rotor blade. It is evident from Fig. 8 that ϵ_w increases with an increase in rotation at all the chordwise and radial locations. It increases almost 50% at the trailing edge of the pressure surface when the speed is doubled. This results in a decrease in the momentum thickness, which is caused by the large migration of the boundary layer toward the tip. It should be emphasized here that this boundary-layer migration will have a drastic effect on the flow near the tip. Even though the momentum thickness is reduced near the midradius, it will increase considerably toward the tip.

The rotation effects have a much more severe impact on the limiting streamline angle on the suction surface (not shown). The value of ϵ_w is almost doubled for a corresponding increase in the rotation. Surprisingly, θ_{11} does not show a corresponding decrease. When the speed is doubled, the

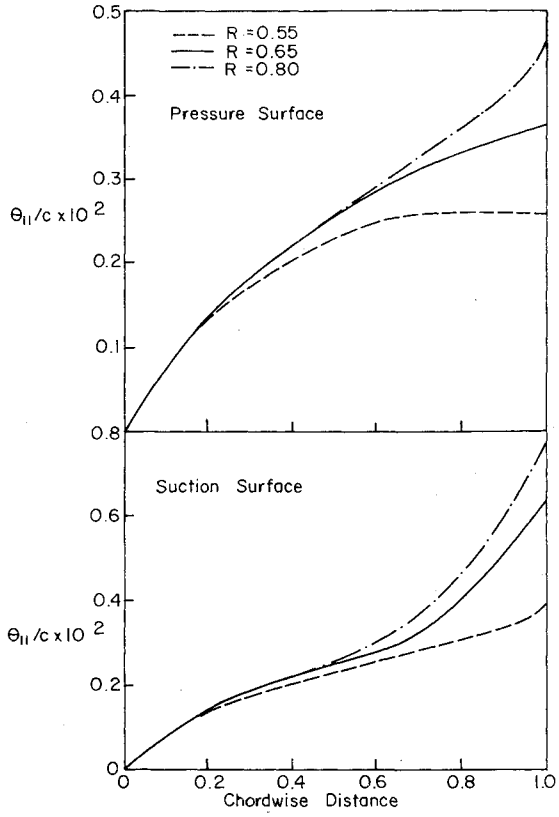

Fig. 10 Predicted chordwise distribution of momentum thickness on a fan rotor blade at various radii.

momentum thickness decreases only by 25%. This discrepancy between the behavior of the two surfaces of the blade for the effects of rotation may be due to the fact that the absolute magnitude of limiting streamline angle on the suction side is much lower than those on the pressure side. Nevertheless, these results are of great significance because the analysis indicates significant differences between a low-speed and a high-speed rotor. In a high-speed rotor, the three-dimensional effects are considerably higher and the boundary layers tend to be thinner than in a corresponding low-speed rotor.

Effect of the Chordwise Pressure Gradient

The effect of the chordwise pressure gradient on the boundary-layer development of a rotor blade was studied using the compressor rotor described earlier as the test case. All the parameters, except the chordwise pressure gradient ($\partial U_e/\partial s$), were held constant. This test case is listed as item 9 in Table 1. The effect of the chordwise pressure or velocity gradient on momentum thickness is well known. Its effect on the limiting streamline angle is shown in Fig. 9. It is evident that as the chordwise pressure gradient is increased, the value of the limiting streamline angle also increases. The increase in ϵ_w due to a higher pressure gradient is not as pronounced as those indicated in Fig. 8, where the rotation effects are studied. Thus it is evident that larger pressure gradients induce appreciable three-dimensionality in rotor boundary layers, increasing both θ_{11} and ϵ_w.

Axial Flow Fan Rotor Blade [18,19]

Extensive measurement of the wake, including one axial station close to the trailing edge of a rotor blade, was carried out by Reynolds and Lakshminarayana.[18] Some of this data and the unpublished information[19] are utilized for comparison with the prediction from the analysis of the authors.

The fan rotor consisted of 12 blades of symmetrical profile, with a blade chord of 15.2 cm and a tip diameter of 0.546 m. This isolated rotor was operated in air and the measurements

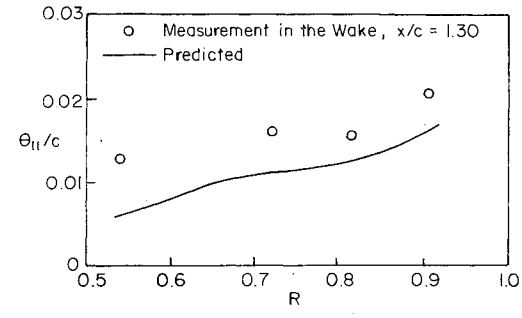

Fig. 11 Measured and predicted total momentum thickness at the trailing edge of a fan rotor blade. [18,19]

were taken with a three-sensor hot-wire probe utilizing the ensemble-averaging technique. Some relevant parameters are listed in item 10 of Table 1, and a detailed description is given in Ref. 18. The blade was operated at a 10-deg incidence.

The predicted chordwise distribution of the momentum thickness at three radii for this case is shown in Fig. 10. The flow is assumed to be turbulent from the leading edge. Substantial radial variation in the momentum thickness is evident. The values of θ_{11} at the trailing edge of the suction surface is almost twice as much as that on the pressure side. The increase in momentum thickness near the trailing edge of the suction surface is much more rapid than those on the pressure side.

The predicted values of the limiting streamline angle ($\epsilon_w = \tan\alpha_w$) at various chordwise and radial locations are similar to that shown in Fig. 7 for the axial compressor rotor. Since this rotor was operated at off-design conditions, the limiting streamline angles were found to be large, indicating severe three-dimensionality in the flow.

The wake data near the rotor trailing edge ($x = 1.3$ at midradius) are shown compared with the predictions in Fig. 11. The value of θ_{11}/C plotted is the total momentum thickness at the trailing edge, the sum of their values on the pressure and the suction surfaces of the rotor blade. The predicted values are lower than the measured values, but the trend is predicted accurately. The momentum thickness increases substantially from hub to tip as predicted from the analysis. The discrepancy between the data and the prediction may have been caused by the fact that the momentum thickness is derived from the wake data at 0.3 chord downstream (as compared to 0.0104 chord downstream for the compressor case).

Conclusions

The momentum integral technique for the analysis of the rotor blade boundary layer has been extended to include Head's entrainment equation as a closure model. The improved technique, the numerical method, and the boundary conditions show good agreement between the measured and the predicted momentum thickness for a wide variety of turbomachinery configurations—cascades, fan and compressor rotors, and axial flow inducer. The method does not include the effects of the annulus wall and the hub wall boundary layers, and hence is not accurate at the tip and hub regions of a rotor. Some of the major conclusions are as follows.

1) The boundary-layer growth on both the accelerating (turbine) and decelerating (compressor) cascade can be predicted accurately. The method is inaccurate beyond the flow separation point.

2) The analysis is accurate for the prediction of the rotor boundary-layer growth, where the effects of both the Coriolis and the centrifugal forces are present. The predicted and measured values of the momentum thickness and the limiting streamline angle show good agreement for the inducer rotor at most of the radial and chordwise locations.

3) Higher momentum thickness on the suction side as compared to the pressure side is predicted for both the compressor and the fan rotor blades.

4) The analysis indicates that the momentum thickness and the limiting streamline angle increase from hub to tip for both the fan and the compressor rotors.

5) The values of the momentum thickness for the compressor and the fan rotor blades, derived from the wake measurement, show good agreement with the predictions.

6) A parametric study of the effects of rotation indicate that when all the other parameters are held constant, the momentum thickness decreases and the limiting streamline angle increases near the midradius with an increase in the rotation.

7) An increase in chordwise pressure gradient, when all other parameters are held constant, increases both the momentum thickness and the limiting streamline angle for a rotor blade.

8) The momentum thickness increases rapidly for the off-design operation of the rotor.

Acknowledgment

This work was supported by NASA through Grant NSG 3266, with P. M. Sockol as the technical monitor.

References

[1]Cumpsty, N. A. and Head, M. R., "The Calculation of Three-Dimensional Turbulent Boundary Layers (1) Flow Over the Rear of an Infinite Swept Wing," *Aeronautical Quarterly,* Vol. 18, Feb. 1967, p. 60.

[2]Thompson, B. G. J. and MacDonald, A. G. J., "The Prediction of Boundary Layer Profile Development for Infinite Yawed Wings," British ARC CP No. 1307, May 1973.

[3]Smith, P. D., "Calculation Methods for Three Dimensional Boundary Layers," British ARC R & M 3523, Dec. 1966.

[4]Mager, A., "Generalization of Boundary Layer Momentum Integral Equations to Three-Dimensional Flow Including Those of Rotating Systems," NACA Rept. 1067, 1952.

[5]Lakshminarayana, B., Jabbari, A., and Yamaoka, H., "Turbulent Boundary Layer on a Rotating Helical Blade," *Journal of Fluid Mechanics,* Vol. 51, Feb. 1972, pp. 545-570.

[6]Anand, A. K. and Lakshminarayana, B., "Three-Dimensional Turbulent Boundary Layer in a Rotating Helical Channel," *Journal of Fluids Engineering,* Vol. 97, No. 2, June 1975, p. 197.

[7]Anand, A. K. and Lakshminarayana, B., "Experimental and Theoretical Investigation of Three-Dimensional Turbulent Boundary Layers and Turbulent Characteristics Inside an Axial Flow Inducer Passage," NASA CR 2888, Aug. 1977.

[8]Katsanis, T. and McNally, W. D., "Revised Fortran Program for Calculating Velocities and Streamlines on the Hub-Shroud Mid-Channel Stream Surface of an Axial-, Radial-, or Mixed-Flow Turbomachine or Annular Duct," NASA TN D-8430, March 1977.

[9]Ludwieg, H. and Tillmann, W., "Untersuchungen uber die Wandschubspannung in Turbluenten Reibungsschichten," *Ingenieur-Archiv,* Vol. 17, 1949, p. 288.

[10]Kline, S. J., Morkovin, M. V., Sovran, G., and Cockrell, D. J., eds., *Proceedings of Turbulent Boundary Layer - AFSOR-IFP,* Stanford Conference, Vol. 1, Stanford University, 1968.

[11]Head, M. R., "Entrainment in Turbulent Boundary Layers," British ARC R & M 3152, Sept. 1958.

[12]Nash, J. F. and Patel, V. C., *Three Dimensional Turbulent Boundary Layers,* Scientific and Business Consultants Inc., Atlanta, 1972.

[13]Peterson, C. R., "Boundary Layer on an Airfoil in a Cascade," Gas Turbine Laboratory, Massachusetts Institute of Technology, Cambridge, Mass., Rept. No. 49, Dec. 1958.

[14]Bammert, K. and Sandstede, H., "Measurements of the Boundary Layer Development Along a Turbine Blade with Rough Surfaces," ASME Paper 80-GT-40, ASMC Gas Turbine Conference and Products Show, New Orleans, March 1980.

[15]Banks, W. H. H. and Gadd, G. E., "A Preliminary Report on Boundary Layers on Screw Propellers and Simpler Rotating Bodies," National Physical Laboratory, England, Rept. SH R27/62, 1962.

[16]Lakshminarayana, B., "An Axial-Flow Compressor Facility Designed for Flow Measurement in Rotor Passages," *Journal of Fluids Engineering,* Vol. 102, Dec. 1980, pp. 402-411.

[17]Ravindranath, A. and Lakshminarayana, B., "Mean Velocity and Decay Characteristics of the Near- and Far-Wake of a Compressor Rotor," *Journal of Engineering for Power,* Vol. 102, No. 3, July 1980, pp. 535-548; also, NASA CR 159518, June 1980.

[18]Reynolds, B. and Lakshminarayana, B., "Characteristics of Lightly Loaded Fan Rotor Blades," NASA CR 3188, Oct. 1979.

[19]Reynolds, B., private communication, 1980.